

In Situ Electrophysiological Examination of Pancreatic α Cells in the Streptozotocin-Induced Diabetes Model, Revealing the Cellular Basis of Glucagon Hypersecretion

Ya-Chi Huang,¹ Marjan S. Rupnik,² Negar Karimian,¹ Pedro L. Herrera,³ Patrick Gilon,⁴ Zhong-Ping Feng,⁵ and Herbert Y. Gaisano^{1,5}

Early-stage type 1 diabetes (T1D) exhibits hyperglucagonemia by undefined cellular mechanisms. Here we characterized α -cell voltage-gated ion channels in a streptozotocin (STZ)-induced diabetes model that lead to increased glucagon secretion mimicking T1D. GYY mice expressing enhanced yellow fluorescence protein in α cells were used to identify α cells within pancreas slices. Mice treated with low-dose STZ exhibited hyperglucagonemia, hyperglycemia, and glucose intolerance, with 71% reduction of β -cell mass. Although α -cell mass of STZ-treated mice remained unchanged, total pancreatic glucagon content was elevated, coinciding with increase in size of glucagon granules. Pancreas tissue slices enabled in situ examination of α -cell electrophysiology. α cells of STZ-treated mice exhibited the following: 1) increased exocytosis (serial depolarization-induced capacitance), 2) enhanced voltage-gated Na^+ current density, 3) reduced voltage-gated K^+ current density, and 4) increased action potential (AP) amplitude and firing frequency. Hyperglucagonemia in STZ-induced diabetes is thus likely due to increased glucagon content arising from enlarged glucagon granules and increased AP firing frequency and amplitude coinciding with enhanced Na^+ and reduced K^+ currents. These alterations may prime α cells in STZ-treated mice for more glucagon release per cell in response to low glucose stimulation. Thus, our study provides the first insight that STZ treatment sensitizes release mechanisms of α cells. *Diabetes* 62:519–530, 2013

Glucagon promotes glucose mobilization in liver through glycogenolysis and gluconeogenesis (1,2). Low blood glucose level normally triggers glucagon release from pancreatic α cells to prevent hypoglycemia caused by physical activity or excessive insulin actions (1–3). In type 1 diabetes (T1D), glucagon secretion becomes dysregulated. In early stage of T1D, α cells hypersecrete (1,2,4), causing excessive release of glucose, resulting in hyperglycemia and leading to long-term complications (blindness and organ failure). As diabetes progresses, α cells suffer from “hypoglycemic blindness,” becoming sluggish in response to low glucose, exacerbating life-threatening acute hypoglycemic episodes

(3,5). No effective treatment has been developed to regulate glucagon secretion to combat hypoglycemic attacks.

Despite the importance of α cells in health and diabetes, this islet cell type has been relatively less studied than β cells. The primary reason for the slower investigation of α cells has been the low-yield isolation (~20% of islet cells) and unreliable and inefficient identification of α cells when using conventional strategies of islet isolation and dispersion. We have recently developed the pancreas slice preparation to effectively circumvent these long-standing technical difficulties in assessing α -cell function (6), allowing reliable, efficient, and immediate examination of living α cells. Islet architecture within slices is well preserved, wherein α cells are retained in their cellulo-social environment, unperturbed by enzymatic and mechanical stresses inherent in conventional α -cell isolation procedures. α cells in pancreas slices were directly assessed via patch pipette. We demonstrated that every single α cell examined exhibited all the classical electrophysiological features of mouse α cells (6).

Although we and others have characterized normal α -cell biology in healthy rodent and human islets in some detail (6,7), disruptions of α -cell biology caused by T1D have been minimally investigated. This is because T1D islets shrink in size and lose their compact islet architecture from immune-mediated β -cell ablation. This has rendered isolation of α cells from immunologically damaged islets by conventional methods technically unfeasible, thus hampering investigation of the α cell in its native disease state. We have now surmounted this problem by using the pancreas slice preparation in mice administered streptozotocin (STZ), which creates a state that in several aspects resembles T1D (8,9). We used GluCre-ROSA26EYFP (GYY) mice, which express enhanced yellow fluorescence protein (EYFP) in α cells (10), to precisely identify α cells within the much reduced islet mass in the pancreas slice. α Cells within pancreas slices can be directly assessed by standard patch-clamp technique. Our combinatorial strategy allowed efficient investigation of α cells in disease (T1D) states that was not previously possible. We elucidated the alterations in ion channel properties in α cells that contribute to the intensified action potential (AP) firing and increased amplitude, which we postulate to lead to the clinically observed systemic hyperglucagonemia in early stage of T1D.

RESEARCH DESIGN AND METHODS

Animal care and all procedures were approved by the Institutional Animal Care and Use Committee of the University of Toronto. GYY mice were previously described by P.G. (10). GYY mice (16–20 weeks old) used in this study were of similar age at which NOD mice develop overt diabetes (11) and have fully developed pancreas with adult-size islets to ensure that islet shrinkage from STZ-induced β -cell death (9) remains visible within the pancreas slices.

From the ¹Institute of Medical Science, University of Toronto, Toronto, Ontario, Canada; ²Faculty of Medicine, Institute of Physiology/CIPKEBIP, University of Maribor, Maribor, Slovenia; ³Cell Physiology & Metabolism, University of Geneva, Geneva, Switzerland; ⁴Pole d'Endocrinologie, Diabète et Nutrition, Université Catholique de Louvain, Brussels, Belgium; and ⁵Physiology and Medicine, University of Toronto, Toronto, Ontario, Canada. Corresponding author: Herbert Y. Gaisano, herbert.gaisano@utoronto.ca.

Received 11 June 2011 and accepted 28 July 2012.
DOI: 10.2337/db11-0786

© 2013 by the American Diabetes Association. Readers may use this article as long as the work is properly cited, the use is educational and not for profit, and the work is not altered. See <http://creativecommons.org/licenses/by-nc-nd/3.0/> for details.

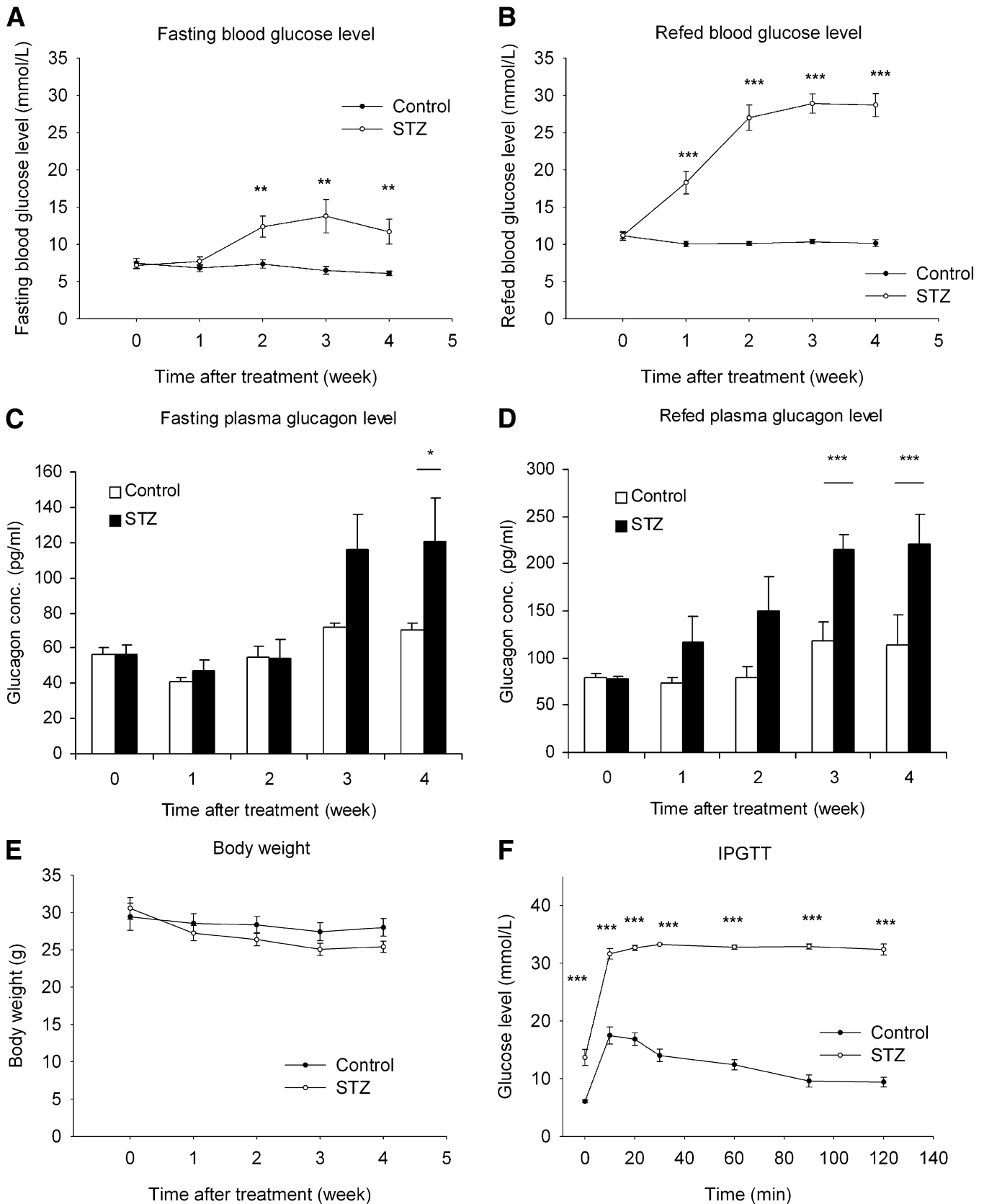


FIG. 1. STZ-induced diabetes in GYY mice. Time courses of fasting (A) and refeed (B) blood glucose levels, fasting (C) and refeed (D) plasma glucagon levels, and body weight (E). The measurements were made periodically from the control and STZ-treated mice before (0 week) and over the course of 4 weeks after the first day of STZ injection. All data are plotted as means ± SEM. **P* < 0.05, ***P* < 0.01, ****P* < 0.001 (control mice, *n* = 10; STZ-treated mice, *n* = 12). F: Time course of IPGTT. Blood glucose levels were measured from the control (*n* = 10) or STZ-treated (*n* = 16) mice 4 weeks postinjection (****P* < 0.001). Conc., concentration.

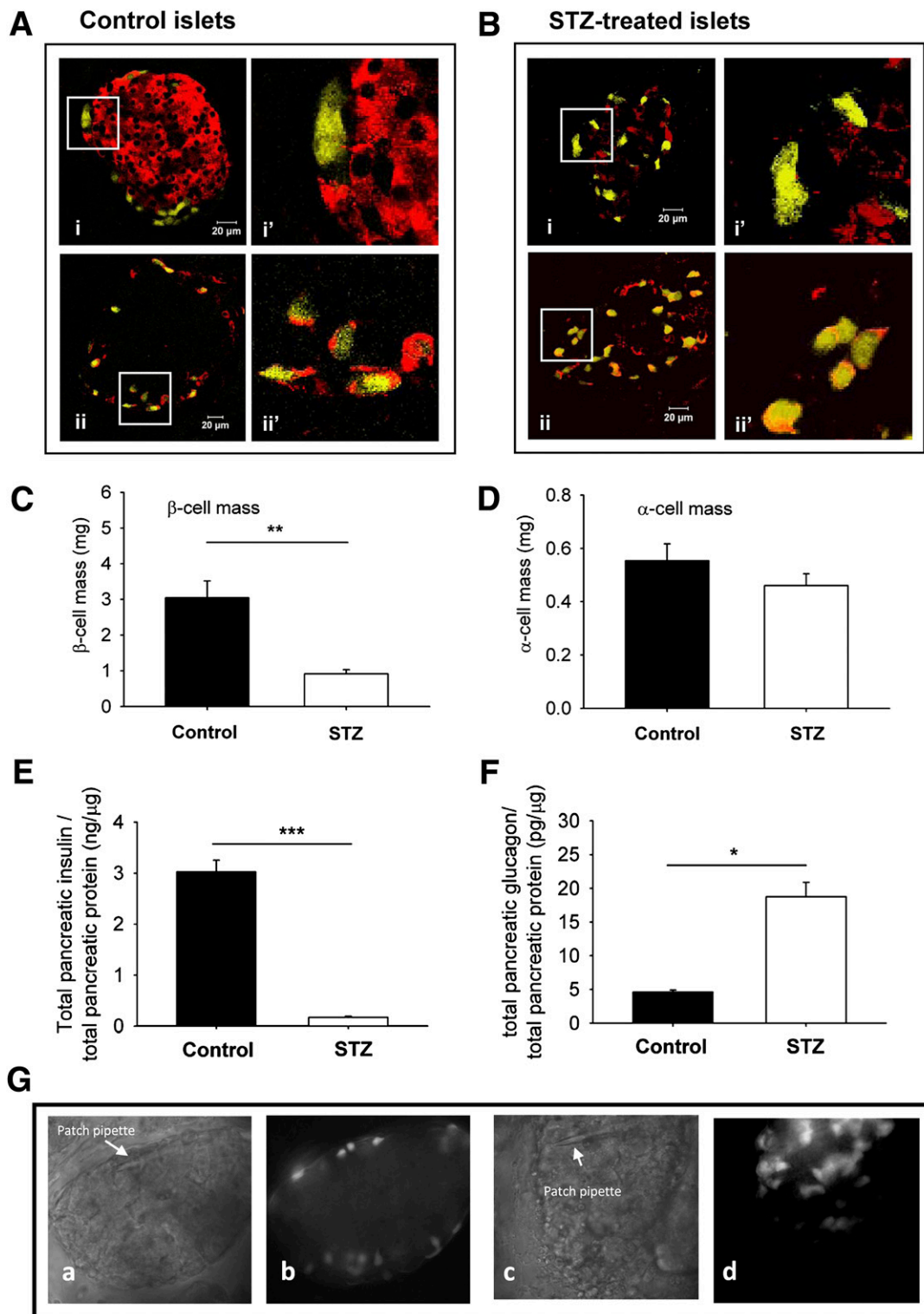


FIG. 2. Comparison of islet morphology between control and STZ-treated GYY mice. **A** and **B**: Representative images of islets of control (**A**) and STZ-treated (**B**) GYY mice embedded in pancreas slices. Images in the *right panels* (*Ai'*, *Aii'*, *Bi'*, and *Bii'*) were magnified from the inset white boxes in the *left panels* (*Ai*, *Aii*, *Bi*, and *Bii*). In control islets (**A**), α cells expressing EYFP (in the cytosol) stained with glucagon located in the periphery of the cells (*Aii* and *Aii'*: red, glucagon; yellow, EYFP). Insulin-labeled β cells (*Ai* and *Ai'*: red, insulin; yellow, EYFP) with α cells redistributed to the islet core (*Bii* and *Bii'*: red, glucagon; yellow, EYFP). Similar to control islets, these α cells in STZ-treated mice expressing EYFP also exhibit glucagon staining in the periphery of the cells. ($n = 5$ mice in each group.) **C** and **D**: Total pancreatic β -cell (**C**) and α -cell (**D**) masses in the control and STZ groups determined 4 weeks after injection ($n = 5$ mice in each group). **E** and **F**: Total pancreatic insulin (**E**) and glucagon (**F**) content in the control and STZ groups measured at 4 weeks after STZ treatment. (* $P < 0.05$, ** 0.01 , and *** 0.001 , respectively; $n = 5$ mice in each group.) **G**: Representative images of pancreas slice prepared from control (**a** and **b**) and STZ (**c** and **d**) mice viewed under bright-field (**a** and **c**) or EYFP-specific (**b** and **d**) filter. In both islets, a patch pipette (white arrow) is shown approaching a cell on the islet edge, which expresses EYFP. (A high-quality digital representation of this figure is available in the online issue.)

Diabetes induction. STZ (Bioshop, Burlington, Ontario, Canada) dissolved in sodium citrate buffer at a single daily dose of 40 mg/kg body mass was injected intraperitoneally into mice for 5 consecutive days and maintained for 4 weeks to allow animals to reach and surpass the peak incidence of β -cell apoptosis (9). Control animals were injected with citrate buffer. Mice were killed by cervical dislocation after the 4th week of STZ treatment for further experimentation.

For the intraperitoneal glucose tolerance test (IPGTT), 1.5 g glucose/kg body wt i.p. was injected into overnight-fasted (16 h) mice; blood glucose (glucometer, LifeScan, Burnaby, British Columbia, Canada) and glucagon were measured as indicated. For refeed levels, mice fasted overnight (for fasting levels) were fed ad libitum with standard normal chow for 3 h. Blood samples were collected from femoral vein and loaded into capillary tubes coated with Kalium-EDTA (Microvette CB 3000; Sarstedt, Montreal, Quebec City, Canada); plasma was separated by centrifugation (10,000g, 10 min), and glucagon was assayed by RIA (Millipore, Etobicoke, Ontario, Canada).

Pancreatic α - and β -cell mass and insulin and glucagon content measurements. Islet cell mass was measured as previously described (12). Briefly, resected pancreata were fixed in 4% paraformaldehyde, embedded in paraffin, and thinly sectioned (5 μ m thin) and then dewaxed, rehydrated, and immunostained with rabbit polyclonal anti-insulin (1:200; Biomedica) or anti-glucagon (1:150; Vision Biosystems) antibodies and counterstained with hematoxylin-eosin. Slides were digitized on a bright-field scanner ($\times 20$ magnification), and quantitative analysis of stained areas was performed with ImageScope software (Aperio Technologies, Vista, CA) using a positive-pixel count algorithm.

For hormone content measurements, isolated pancreata were placed in acid-ethanol mixture (1.5% HCl, 70% EtOH), incubated overnight (-20°C), and then homogenized; the tissue levels of insulin and glucagon extracted by centrifugation (5,000g, 15 min) were then determined by RIA kits (Millipore) and normalized to total pancreatic protein content.

Pancreas slice preparation. Pancreas tissue slices were prepared as we recently reported (6). Electrophysiology was conducted an hour after preparation and completed within 5 h.

Immunofluorescence and electron microscopy. Immunofluorescence microscopy was performed as described in our recent report (6) with the following primary antibodies (1:100; 3 h): mouse anti-glucagon or anti-insulin (Sigma) or anti-somatostatin (GeneTex, Irvine, CA). Electron microscopy was performed as we previously described (13). Glucagon granules (thus α cells) were identified by the typical appearance (large black dense core with thin halo) (14,15). Glucagon dense core diameter was measured using NIH ImageJ software.

Electrophysiology. Electrophysiological recording was done as we described in our recent report using pancreatic slices (6), and here EYFP-expressing islet α cells in slices can be visualized and patched on. Standard whole-cell configuration was applied to all recordings, using a lock-in patch-clamp amplifier (EPC-9; HEKA Elektronik, Lambrecht/Pfalz, Germany). The signals were low-pass filtered and stored on the computer. Pulse (HEKA Elektronik) was used for voltage pulse generation, data acquisition, and basic analysis, followed by further processing of the acquired data using Igor software. Voltage-clamp mode was used for recording all currents, and current-clamp mode was used for recording membrane potentials. The resting membrane potential was determined immediately after current-clamp mode was made, and spontaneous APs were observed without any current injection. The number of APs over recording periods of 30–120 s was counted using the event detection/threshold search program of Clampfit9 software (Axon), with a threshold range between -28.6 and -29.6 mV. The amplitude and firing frequency of APs were analyzed using Clampfit9 software. The firing frequency was normalized and presented as the number of APs per second (Hz). The extracellular solution has previously been described (6). The pipette solutions used were as follows: 1) for recording Ca^{2+} and Na^{+} currents, in millimoles, 127 Cs-methanesulfonate, 8 CsCl, 10 HEPES, 20 tetraethylammonium-Cl, 2 MgCl_2 , 2 Na_2ATP , and 0.05 EGTA; 2) for recording K^{+} current and depolarization-evoked cumulative membrane capacitance (ΔC_m), in millimoles, 140 KCl, 10 HEPES, 2 MgCl_2 , 2 Na_2ATP , and 0.05 EGTA; and 3) for membrane potential recording, the same pipette solution was used as in no. 2. pH of all solutions was 7.2; osmolality was 300 ± 10 mOsm kg^{-1} . All recordings were performed at 32°C . The pipette resistance ranged between 2 and 4 M Ω . All chemicals were from Sigma.

RESULTS

STZ induction of diabetes in GYY mice. Fasting blood glucose level in STZ-treated GYY mice increased at 2 weeks (Fig. 1A) and refeed blood glucose level at 1 week (Fig. 1B) posttreatment. Fasting (Fig. 1C) and refeed (Fig. 1D) plasma glucagon levels rose to abnormal levels at 3 weeks and 1 week post-STZ treatment, respectively. The increased plasma glucagon levels (Fig. 1C and D) contributed in part

to the observed hyperglycemia (Fig. 1A and B) in STZ-treated GYY mice. At 4 weeks post-STZ treatment, the mice showed the stable diabetes phenotype characterized as high and sustained fasting blood glucose (Fig. 1A) (control 6.1 ± 0.3 mmol/L, $n = 10$, vs. STZ 11.7 ± 1.7 mmol/L, $n = 12$), refeed blood glucose (Fig. 1B) (control 10.1 ± 0.5 mmol/L vs. STZ 28.7 ± 1.5 mmol/L), fasting plasma glucagon (Fig. 1C) (control 70.3 ± 4.3 pg/mL vs. STZ 120.9 ± 24.2 pg/mL), and refeed plasma glucagon (Fig. 1D) (control 113.9 ± 31.8 pg/mL vs. STZ 220.1 ± 32.7 pg/mL) compared with the controls. The STZ-GYY mice also experienced mild weight loss (Fig. 1E) and developed glucose intolerance (IPGTT) (Fig. 1F) at 4 weeks after treatment. We thus selected mice at 4 weeks post-STZ treatment for all the subsequent in vitro and electrophysiological experiments.

Effects of STZ-induced diabetes on islet morphology, α - and β -cell mass, and glucagon and insulin content.

Confocal microscopy analysis of pancreas slices demonstrated a redistributed pattern of insulin (Fig. 2Bi and Bi' [cells in red]) and glucagon (Fig. 2Bii and Bii' [cells in both red and yellow]) staining in islets of STZ-treated mice compared with controls. Control islets showed glucagon-labeled α cells resided along the islet periphery (Fig. 2Ai and 2Ai' [cells in yellow] and 2Aii and 2Aii' [cells in both yellow and red]) and the larger mass of insulin-labeled β cells occupied the islet core (Fig. 2Ai and Ai', red). Total pancreatic α - and β -cell masses were determined by immunohistochemical quantification of insulin- and glucagon-positive staining areas (see RESEARCH DESIGN AND METHODS), normalized to entire pancreas cross-sectional tissue area; the resulting values were then multiplied by the wet pancreas weight of each mouse. Mean pancreas wet weights were similar (control 0.216 ± 0.006 g vs. STZ mice 0.251 ± 0.05 g; $P = 0.43$). The relative ratio of α cell to total pancreatic tissue area was also similar (control 0.0029 ± 0.0005 vs. STZ 0.0024 ± 0.0002 ; $P = 0.36$). However, the ratio of β cell to total pancreatic tissue area was reduced in STZ-treated mice (control 0.0152 ± 0.0017 vs. STZ 0.0048 ± 0.0006 ; $P = 0.0005$). STZ treatment reduced β -cell mass by 71% (Fig. 2C), but there was no difference in α -cell mass between STZ and control mice (Fig. 2D).

Total pancreatic glucagon and insulin content normalized to the total protein content of each pancreas showed that STZ mice had increased mean pancreatic glucagon content (STZ mice $440,747 \pm 55,473$ pg vs. control $103,398 \pm 5,999$ pg; $n = 5$ mice/group, $P = 0.0002$) and reduced mean insulin content (STZ mice $4,091 \pm 564$ ng vs. control $68,518 \pm 5579$ ng; $P = 0.000003$). Mean pancreatic protein content was similar (STZ mice $23,590 \pm 470$ μ g vs. control $22,621 \pm 473$ μ g; $P = 0.18$). In the STZ-treated mice group, total pancreatic insulin content per protein content was severely reduced because of β -cell destruction (Fig. 2E) (control 3.02 ± 0.22 ng/ μ g vs. STZ 0.17 ± 0.02 ng/ μ g). Surprisingly, total pancreatic glucagon content per protein content in the STZ group was remarkably elevated to fourfold higher than in control mice (Fig. 2F) (control 4.59 ± 0.32 vs. STZ 18.71 ± 2.19 pg/ μ g).

STZ-treated GYY mouse α cells are larger and have larger glucagon granules. The above results demonstrated that STZ induction of diabetes did not alter α -cell mass but increased glucagon content, which taken along with the increased plasma glucagon led us to postulate that each α cell in the STZ-treated mouse islet contains and releases more glucagon. We directly tested this hypothesis by two strategies: 1) single α -cell ΔC_m induced by serial membrane depolarization and 2) ultrastructural analysis of

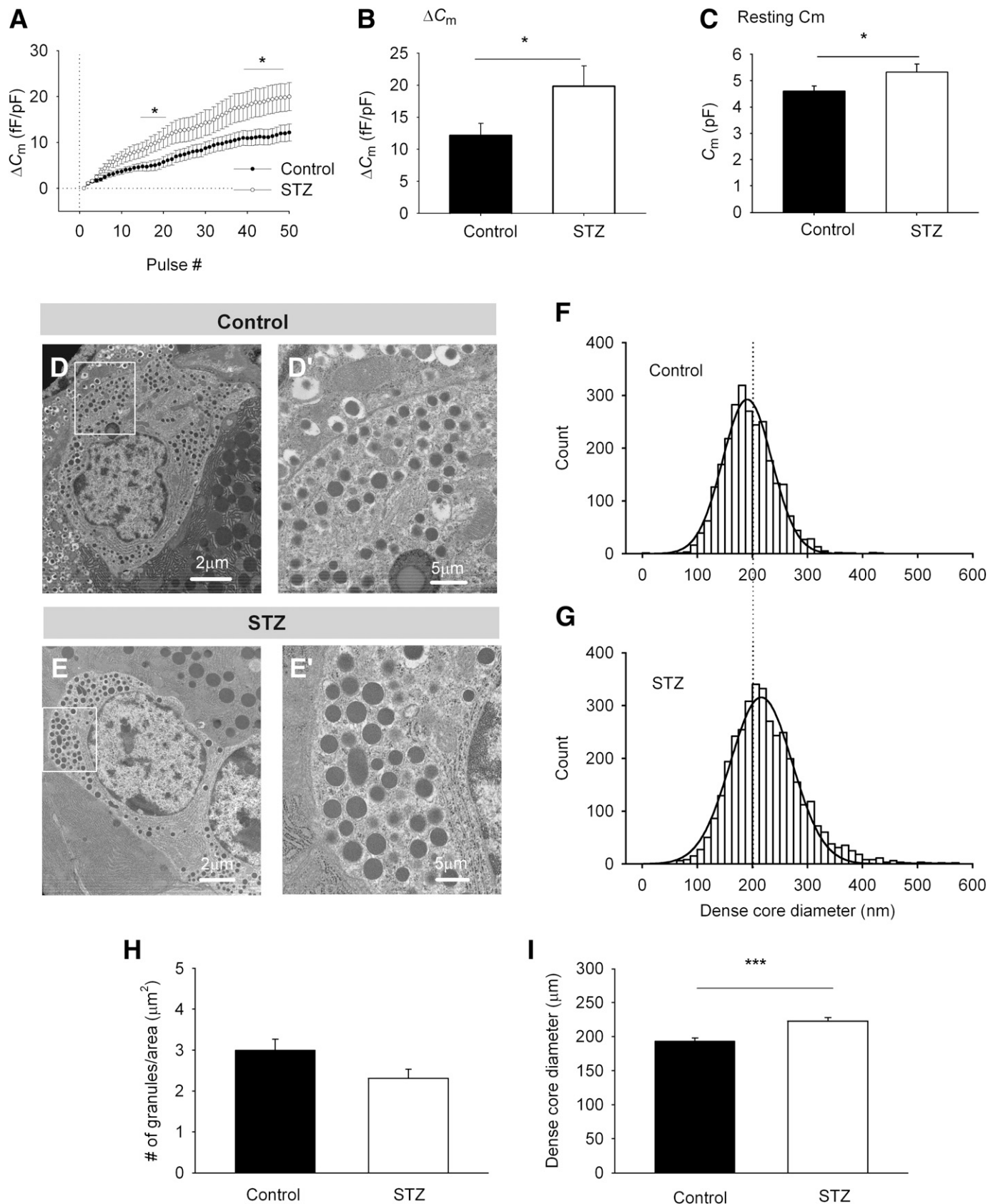


FIG. 3. α -Cell glucagon granule exocytosis in STZ-treated GYY mice. **A:** Mean α -cell capacitance (ΔC_m) triggered by a train of 50 depolarizing pulses from -80 mV (60 ms) to 10 mV (40 ms). $*P < 0.05$; $n = 27$ cells from five control mice (\bullet), $n = 30$ cells from four STZ mice (\circ). For recording conditions, see RESEARCH DESIGN AND METHODS. **B:** ΔC_m elicited by the 50th depolarizing pulses in **A** ($*P < 0.05$; $n = 27$ cells from five control mice, $n = 30$ cells from four STZ mice). **C:** Mean resting C_m of α cell, as a measure of the cell size. $*P < 0.05$; $n = 27$ cells from five control mice, $n = 30$ cells from four STZ mice. **D** and **E:** Representative electron micrographs of α cells of control (**D**) and STZ-treated (**E**) mice. **D'** and **E'**: Magnified images of the white rectangles in **D** and **E**. **F** and **G:** Gaussian distribution curve of glucagon granule dense core diameters of control (**F**) ($n = 2,642$

α -cell glucagon granules. Since GYY mice express EYFP in pancreatic α cells (10,16), this allows α cells to be visualized within pancreas slices under a fluorescence microscope (Fig. 2Gb and Gd) and be accurately reached with the patch pipette (Fig. 2Ga and Gc). We performed electrophysiological characterizations on every recorded α cell as previously reported (6) to further confirm their identity.

A train of depolarizing pulses trigger ΔC_m in α cells due to Ca^{2+} influx and subsequent glucagon granule exocytotic fusion, as an indicator of α -cell secretion (6). Figure 3A shows mean ΔC_m in α cells of control and STZ mice in response to 50 pulses depolarizing from -80 to 10 mV, which was higher in STZ-treated mice α cells. Figure 3B summarizes the cumulative ΔC_m triggered at the 50th pulse to be higher in α cells of STZ-treated mice (control 12.2 ± 1.9 fF/pF vs. STZ 19.9 ± 3.2 fF/pF; $P < 0.05$). Interestingly, the resting C_m of α cells (Fig. 3C) measured before the depolarization stimuli, which is proportional to cell membrane area, was also slightly increased in STZ α cells (5.33 ± 0.3 fF/pF) compared with control α cells (4.61 ± 0.18 fF/pF; $P = 0.0496$).

The increases in both evoked and resting C_m in α cells of STZ-treated mice suggest the possibility of an increase in the number and/or size of glucagon granules fusing with plasma membrane. To assess this possibility, we performed electron microscopy analysis of the islet α cells (Fig. 3D, control α cells; Fig. 3E, STZ-treated α cells). The corresponding enlarged views of the indicated areas (Fig. 3D' and E') show the glucagon dense core granules to be obviously larger in STZ α cells. Quantitative analysis shows that the mean diameter of granule dense core (Fig. 3I) was indeed larger in α cells of STZ-treated mice (228.50 ± 1.17 nm, $N = 3,679$ granules/32 cells; $P < 0.0001$) than control α cells (195.48 ± 0.94 nm, $N = 2,642/18$ cells). Analysis of granule distribution shows a shift in the overall sizes of glucagon granules of STZ-treated mice (Fig. 3G) compared with control α cells (Fig. 3F), with corresponding modes (peak of the curves relative to the vertical dotted line) of 209 ± 1.56 and 184 ± 1.5 nm, respectively. However, the number of glucagon granules per α cell determined as mean glucagon granules/cell area (Fig. 3H) was similar (control 3.0 ± 0.3 granules/ μm^2 vs. STZ 2.3 ± 0.3 granules/ μm^2). If one assumes that dense core granules are perfect spheres and sizes of α cells are similar between the two groups, the volume of glucagon in α cells can be calculated by the equation $V = 4/3 \pi r^3$, where r is the radius of the dense core. Accordingly, the volume of glucagon of an α cell of STZ-treated mice can be estimated to be 1.6 times larger than control α cells. Since resting C_m measurement (Fig. 3C) suggested an increased cell size in STZ-treated α cells, glucagon contained in α cells of STZ-treated mice should be >1.6 times larger than control α cells.

Nonetheless, this increased glucagon content in glucagon granules may not be sufficient to fully account for the four times increase in pancreatic glucagon content in STZ-treated mice. Taken along with the similar sizes of α -cell mass, our results suggest that the excess glucagon content per α cell is likely also contributed by accumulation of glucagon content in other compartments (endoplasmic reticulum, Golgi, etc.), which in turn suggests an increased

in glucagon protein synthesis (which we currently don't have the technical ability to determine).

Voltage-gated K^+ currents. Voltage-gated K^+ (K_V) channels, shown to play a positive role in regulating glucagon secretion (17), were therefore assessed in α cells of control and STZ-treated mice (Fig. 4). In the control group (15 cells), a transient K_V current became detectable when depolarizing membrane potential to -30 mV and above (Fig. 4A [control]); this current inactivated rapidly (~ 30 ms). Further depolarizing the membrane to -20 mV and higher voltages evoked an additional sustained K_V component (indicated in Fig. 4A). In the STZ group (14 cells), α -cell transient K_V current was notably suppressed (Fig. 4A [STZ]). Figure 4B summarized the transient K_V current density, which was significantly suppressed in STZ α cells when membrane potential was depolarized to 20 mV (control 281.8 ± 20.2 pA/pF vs. STZ 241.8 ± 11.4 pA/pF; $P < 0.05$) and higher voltages. Figure 4C summarized K_V -sustained current density, which was comparable between the two groups.

Voltage-gated Ca^{2+} currents. It is possible that α cells in STZ-treated mice might have larger Ca^{2+} influx to in part explain the larger C_m increase. We thus examined whether there is alteration in the properties of Ca^{2+} channels. In all the experiments, tetrodotoxin (0.1 $\mu g/mL$) was added in the bath solution to block voltage-gated Na^+ current. A 300-ms ramp protocol running from -80 to 60 mV was applied to each α cell to trigger low voltage-activated (LVA) and high voltage-activated (HVA) Ca^{2+} currents. α cells from STZ-treated mice possessed LVA and HVA Ca^{2+} current density similar to that of control mouse α cells (Fig. 5A–H) (mean LVA control -3.14 ± 0.51 pA/pF vs. STZ -2.85 ± 0.25 pA/pF, $P > 0.5$; mean HVA control -7.10 ± 1.15 pA/pF vs. STZ -6.84 ± 0.82 pA/pF, $P > 0.5$; $n = 8$ control cells and 16 STZ cells). Since T-type current likely contributes to LVA Ca^{2+} currents, we added NiCl (100 $\mu mol/L$) to block T-type Ca^{2+} channels (Fig. 5A and B [control] and Fig. 5E and F [STZ]). As anticipated, NiCl reduced LVA Ca^{2+} current amplitude in α cells of controls from 3.14 ± 0.51 to 1.87 ± 0.42 pA/pF (Fig. 5A and B) ($n = 6$ cells) and that of STZ-treated mice from 2.51 ± 0.25 to 0.84 ± 0.29 pA/pF (Fig. 5E and F) ($n = 11$ cells). For confirmation of the HVA Ca^{2+} current component, $CdCl_2$, a broad-spectrum HVA Ca^{2+} channel blocker, was applied. The inward current component, peaked at 0 – 10 mV in both control (Fig. 5C and D [$n = 6$ cells]) and STZ (Fig. 5G and H [$n = 6$ cells]) cells, was completely abolished by Cd^{2+} (200 $\mu mol/L$). Taken together, our results indicate that Ca^{2+} current in α cells is contributed by predominantly HVA channels, consistent with previous reports (18,19). Both current amplitudes of HVA- and T-type channels were not significantly altered by STZ treatment.

Voltage-gated Na^+ currents. Current-voltage dependence of voltage-gated Na^+ inward current was assessed by using Cs^{2+} -based tetraethylammonium-containing pipette solution to block K_V currents (Fig. 6A). Na^+ current can be elicited in every α cell of both control and STZ groups from -80 -mV holding potential. Na^+ inward current became detectable when depolarizing membrane potential to higher than -30 mV (Fig. 6A). Dotted lines indicate zero current level. The peaked Na^+ current

granules from 18 cells of three control mice) and STZ-treated (G) ($n = 3,679$ granules from 32 cells of three STZ-treated mice) mice. Mean number of granules (H) and mean dense core diameter (I) of glucagon granules in α cells of control and STZ mice obtained from the same datasets in F and G, respectively. *** $P < 0.001$.

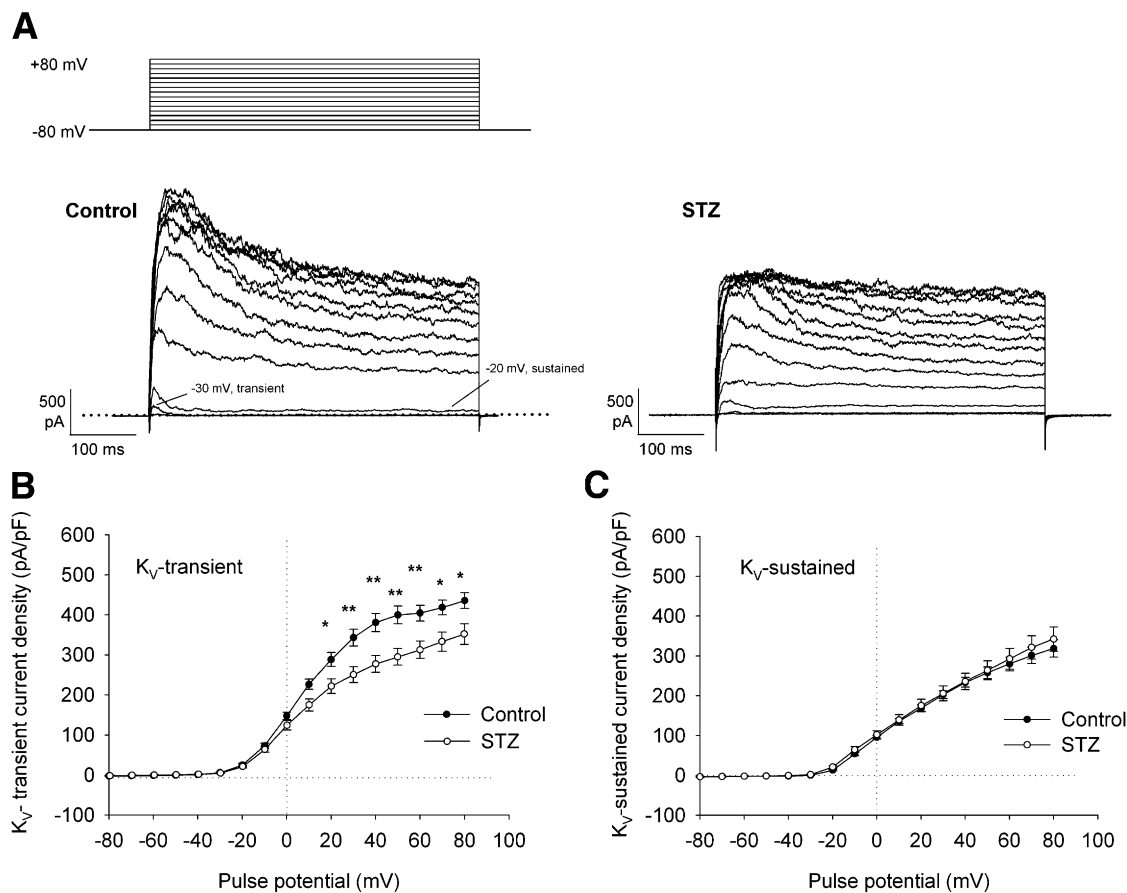


FIG. 4. Voltage-gated K^+ current in α cells of STZ-treated GYY mice. **A:** Representative whole-cell voltage-gated K^+ current traces evoked by a series of 500-ms pulses (*top panel*). *Top panel:* Step-depolarizing protocol from a holding potential of -80 to 80 mV in 10 -mV increments. (For clarity, traces evoked between -70 and -50 mV were not shown.) For recording conditions, see RESEARCH DESIGN AND METHODS. **B** and **C:** Current-voltage (*I-V*) relationships. K_V transient (**B**) (peak current evoked within the first 100 ms) and K_V sustained (**C**) (mean current of the last 100 ms) current density was plotted against the applied voltages ($n = 15$ cells from two control mice, $n = 14$ cells from two STZ-treated mice) ($*P < 0.05$; $**P < 0.01$). Note that the K_V transient current density was reduced in the STZ group at ≥ 20 mV, whereas K_V sustained current density remained similar to that in controls.

amplitudes were -59.6 ± 6.2 pA/pF in controls and -78.4 ± 9.9 pA/pF in the STZ group upon depolarizing to 0 mV (Fig. 6B and C). Na^+ channel *I-V* relationships of both control and STZ α cells exhibited a U-shaped voltage-dependent activation (Fig. 6B). Upon depolarizing to between -20 and 0 mV, α cells of the STZ group revealed significantly larger Na^+ current density than controls ($P < 0.05$). Peak Na^+ current was reached between -10 and 0 mV in both the STZ and control groups. Steady-state Na^+ -channel inactivation was examined by a depolarizing pulse to 0 mV from a set of conditioning pulses between -150 and 0 mV in 10 -mV increments (Fig. 6D). In both control and STZ-group α cells, steady-state Na^+ channel inactivation curve showed no difference; Na^+ channel half-inactivation potential ($V_{1/2}$) in the control and STZ groups was -37.2 and -36.4 mV, respectively (Fig. 6E).

Membrane electrical property of α cells in control and STZ-treated mice. Voltage-gated Na^+ and K^+ currents are important components contributing to α -cell AP firing. We demonstrated that in the STZ-treated group, the Na^+ and K_V current densities are, respectively, increased and decreased, and, thus, AP firing pattern in α cells could be subsequently altered. We performed current-clamp recordings to test this postulation.

After breaking the seal between pipette and cell membrane in voltage-clamp mode, current clamp mode was

immediately switched to record resting membrane potential and regenerative AP firing. To confirm the α -cell type in addition to their cellular EYFP (6), a short step protocol (< 4.5 s) was executed in voltage-clamp mode to determine the Na^+ -channel $V_{1/2}$.

The resting membrane potential in α cells was not significantly different between the two groups (control -56.3 ± 1.4 mV vs. STZ -54.0 ± 2.9 mV) (Fig. 7C). Robust AP firing was recorded in control (Fig. 7A) and STZ-treated mouse α cells (Fig. 7B). In control cells, AP fires spontaneously at a mean firing frequency of 0.68 ± 0.16 Hz (Fig. 7D); initiating at approximately -45 mV, giving rise to mean upstroke amplitude of 33.7 ± 1.8 mV, which then rapidly repolarized (Fig. 7A'). In α cells of STZ-treated mice, AP firing frequency was significantly higher (2.33 ± 0.27 Hz; $P < 0.0001$) (Fig. 7B and D), along with higher mean AP amplitudes (control 33.7 ± 1.8 mV vs. STZ 54.2 ± 2.1 mV, $P < 0.0001$).

DISCUSSION

α Cells in healthy GYY mice expressed voltage-gated Na^+ , Ca^{2+} , and K^+ currents and ΔC_m when depolarized. These electrophysiological properties are comparable with their background C57BL/6J and NMRI mice (6,10), validating GYY mice as an excellent model to study α -cell physiology

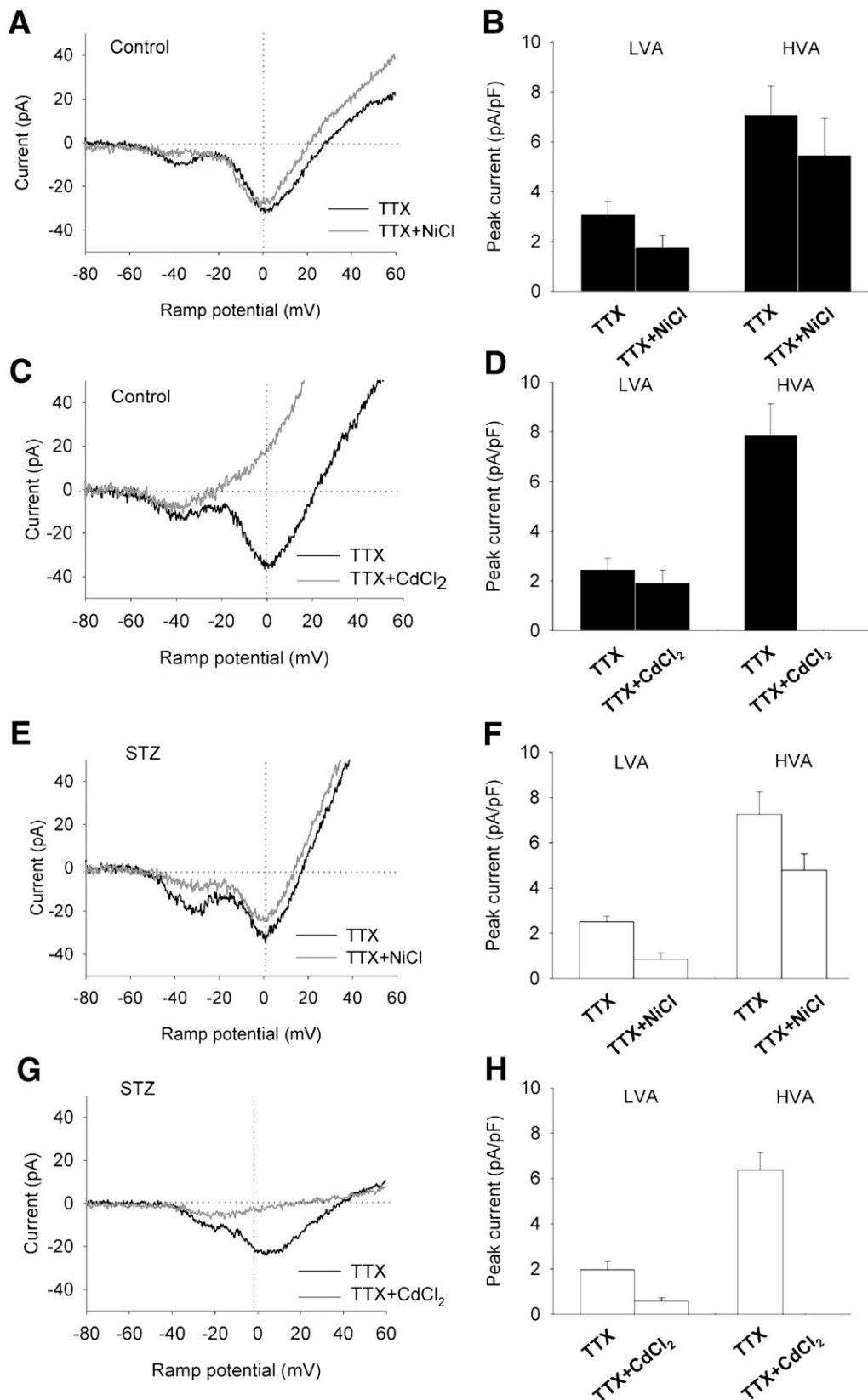


FIG. 5. Voltage-gated LVA and HVA Ca²⁺ current in α cells of STZ-treated GYY mice. Tetrodotoxin (TTX) (0.1 μg/mL) was added to block voltage-gated Na⁺ channels in all recordings. Representative I–V curves evoked by a 300-ms ramp protocol demonstrating LVA (A) and HVA (C) components in control cells. NiCl₂ (100 μmol/L) selectively blocked the LVA component, whereas CdCl₂ (200 μmol/L) blocked HVA components. The data are summarized in B and D. For recording conditions, see RESEARCH DESIGN AND METHODS. Representative I–V curves evoked by the ramp protocol demonstrating LVA (E) and HVA (G) components in STZ-treated cells. The data are summarized in F and H.

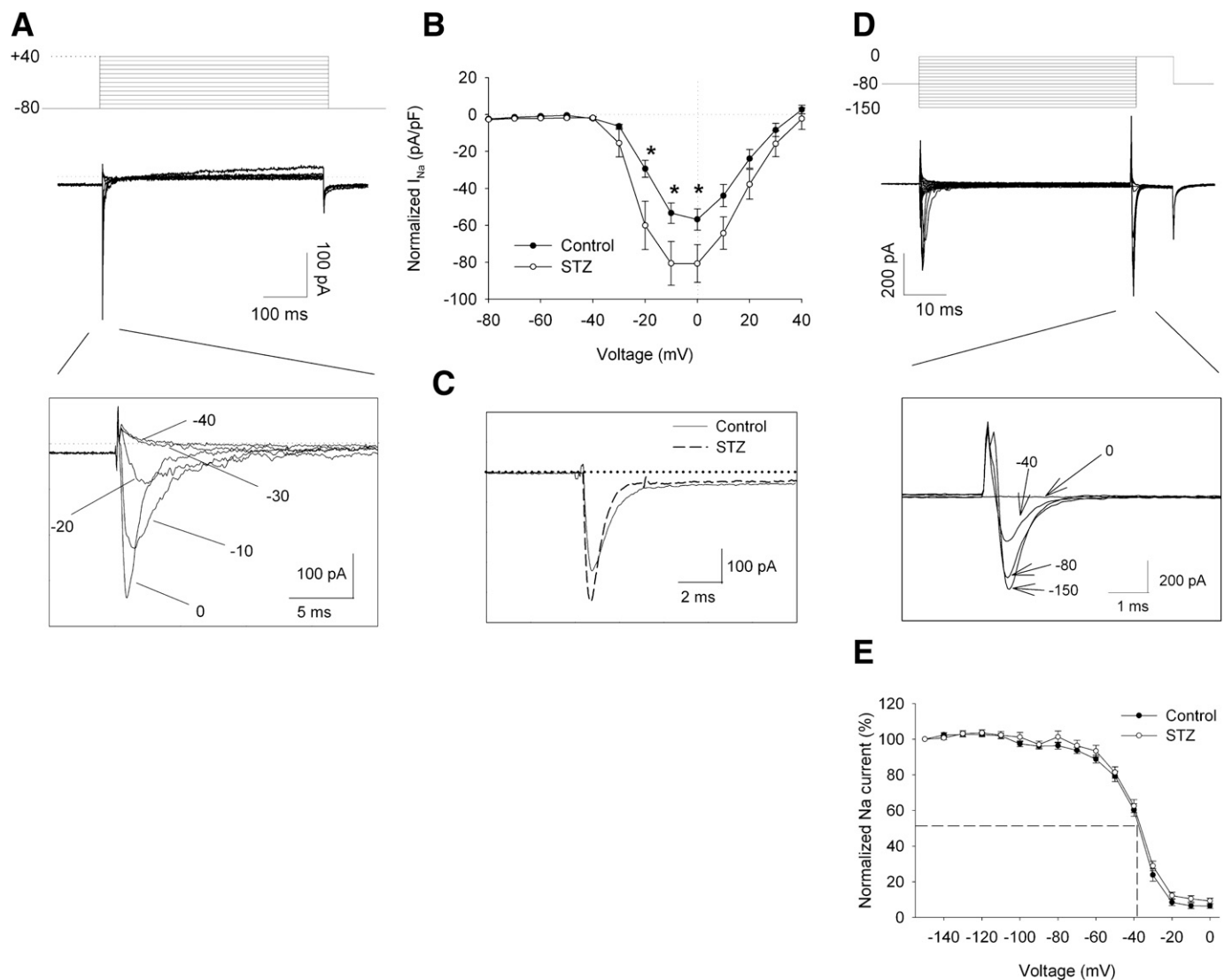


FIG. 6. Voltage-gated Na^+ current in α cells of STZ-treated GYY mice. **A:** Whole-cell Na^+ current. Representative traces of Na^+ current of a control α cell elicited by a 500-ms step depolarizing protocol from -80 to 40 mV in 10 -mV increments at a holding potential of -80 mV (top panel). The magnified Na^+ current in a larger time scale is shown in the inset box. Numbers in the box denote the applied voltage (mV). For recording conditions, see RESEARCH DESIGN AND METHODS. **B:** I-V relationship of the Na^+ current. The peak Na^+ current measured from the cells in the control and STZ groups is presented as the current density and plotted against the applied voltage. The current density was larger in the STZ group at the given voltage pulses. *Difference between the two groups was statistically significant ($P < 0.05$; control, $N = 34$ cells from six mice; STZ, $N = 37$ cells from four mice). **C:** Representative traces of Na^+ current recorded from α cells in the control and STZ groups. The current was elicited by a step pulse from -80 to 0 mV. **D:** Steady-state inactivation properties of the Na^+ channel. Representative current traces of a control cell were elicited by a standard two-pulse protocol (top panel). The magnified Na^+ currents elicited by the test pulses are shown in the inset box. Numbers indicated by arrows in the box denote the test pulse voltage (mV). **E:** Steady-state Na^+ current inactivation curves from control and STZ groups. The $V_{1/2}$ is indicated by dashed lines. No differences were found between the control and STZ groups ($P > 0.05$; control, 34 cells from six mice; STZ, 37 cells from four mice). All of the recording were performed in Na^+ 125 mmol/L in bath solution with Cs^+ (135 mmol/L)-based pipette solution.

and pathophysiology. STZ-treated GYY mouse α cells exhibited hyperglucagonemia and consequent hyperglycemia. Hyperglucagonemia in STZ-treated GYY mice resulted from elevated total pancreatic glucagon content partly contained in the larger glucagon granules, which are expected to effect more stimulated-glucagon granule release. Since total pancreatic α -cell mass of STZ-treated GYY mice remained unchanged while total pancreatic glucagon content was fourfold elevated, it can be predicted that the larger glucagon granules containing some of the excess glucagon are exocytosed in response to every stimulus (i.e., low glucose) on each α cell, culminating in the observed hyperglucagonemia. This is evident by the higher C_m increase in STZ-treated mouse α cells when electrically depolarized. Our results in the STZ-treated mouse are similar

to a recent report showing that genetically induced near-complete β -cell ablation led to increased α -cell glucagon content and also consequent hyperglucagonemia (20).

What are the electrical and/or cellular properties of α cells in STZ-treated mice that contributed to the observed hyperglucagonemia? First, AP firing frequency and amplitude in α cells of STZ-treated mice were more intensified, which would be expected to lead to more glucagon secretion. Whereas these changes in AP are expected to increase Ca^{2+} influx, we showed that whole-cell Ca^{2+} current was not different between STZ-treated and control mice. The increased AP could be attributed to changes in Na^+ and K^+ currents; in fact, STZ-treated mouse α cells exhibited larger Na^+ current density and lower K^+ current

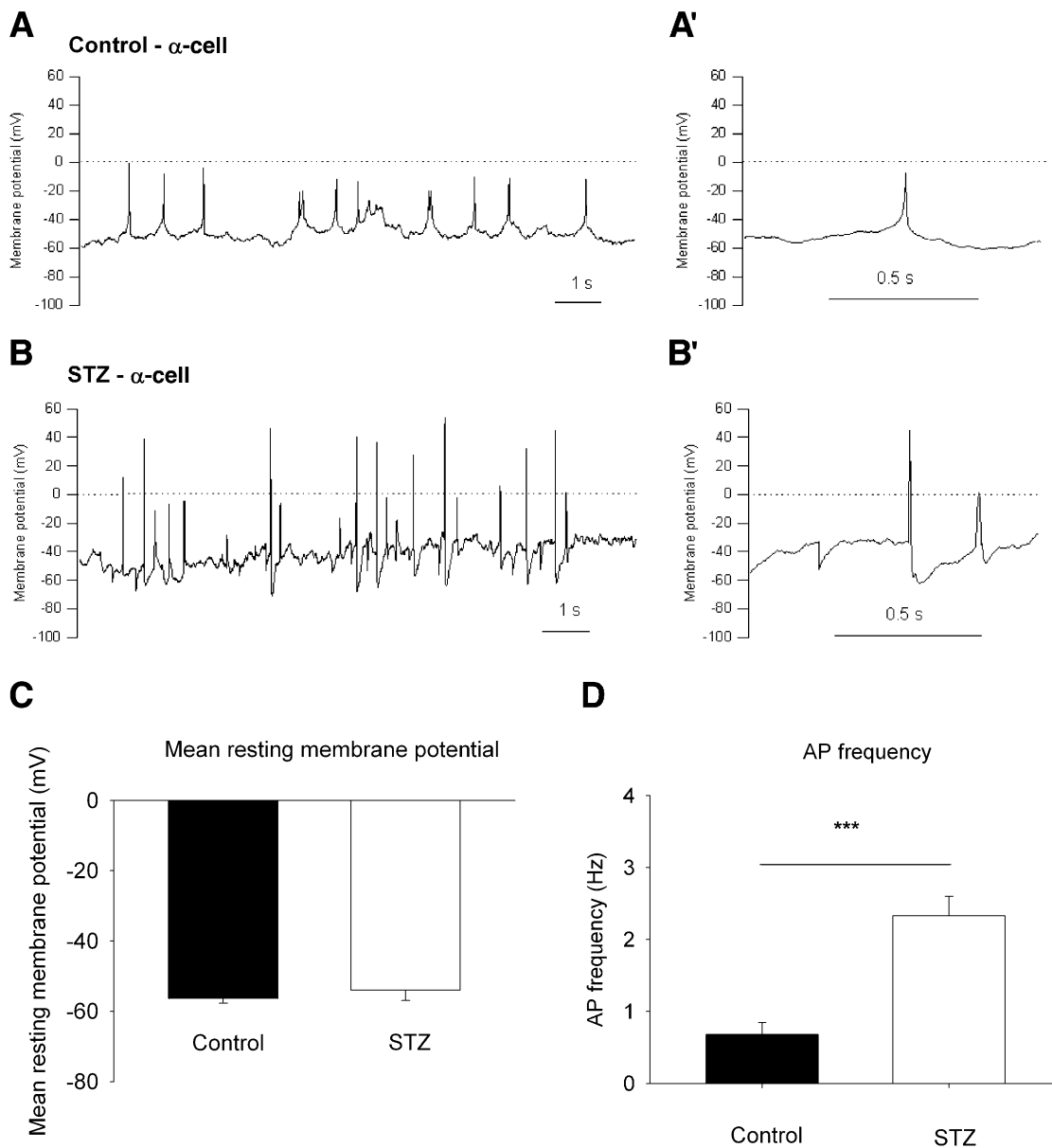


FIG. 7. α-Cell membrane electrical activity of control and STZ-treated mice. **A:** A representative α-cell membrane potential trace of a control mouse by current-clamp recording. For recording conditions, see RESEARCH DESIGN AND METHODS. **A':** A single AP profile in **A** shown in a larger time scale. Dashed line depicts zero current level in all graphs. **B:** A representative α-cell membrane potential trace from an STZ-treated mouse. Note the larger AP amplitudes and more intense frequency of AP firing in the STZ group compared with the control (**A**). **B':** An AP profile in **B** shown in a larger time scale. **C:** Mean resting membrane potential recorded in α cells of control (black bar) and STZ-treated (white bar) mice. The data are presented as means ± SEM. ($P > 0.05$; 19 cells of seven control mice and 34 cells of four STZ-treated mice.) **D:** Summary of α-cell AP firing frequency between control and STZ-treated mice. The mean ± SEM firing frequency increased significantly in the STZ group (15 cells from seven control mice and 27 cells from three STZ-treated mice, $***P < 0.001$).

density (discussed below). Second, the higher C_m increase in STZ-treated mouse α cells induced by serial membrane depolarization can be attributed to the larger glucagon granules exocytosing at the same Ca^{2+} stimulus, thus emptying a larger cargo of glucagon than control mouse α cells. We showed that K_V transient current within healthy α cells is rapidly activated and inactivated, which is similar to the A-type K current we (19) and Rorsman and colleagues (21) have previously demonstrated in rodent α cells. Consistent with the consensus thinking, this would suggest that the reduced K_V transient current in α cells of STZ-treated mice was likely the A-type K current, contributing to the observed increased AP firing rate and amplitude (21,22). However, recent reports showed that

the K_V transient currents in both α- and β cells could also be contributed by large-conductance Ca^{2+} -activated voltage-gated K^+ currents (BK currents) (7,23,24), and, hence, reduced BK currents could also contribute to increased secretion and potentiated AP amplitude (7,20,21,25). In STZ-treated mouse α cells, we noted the increased Na^+ current density coincided with an increase in AP amplitude. As expected (7,21), tetrodotoxin (an Na^+ -channel blocker) inhibited glucagon secretion in both STZ and control pancreas slices (data not shown). These findings are consistent with the notion that Na^+ current influx-evoked AP trigger glucagon granule exocytosis.

What are the factors in STZ-treated mice that would cause suppression of K_V -transient current and enhancement

of Na⁺ current in α cells? One possibility is the loss of paracrine regulation emanating from β -cell destruction, and these paracrine factors include insulin, γ -aminobutyric acid, and zinc (26–30) and possibly other factors. A second possibility is inflammatory cytokines secreted by cytotoxic T cells recruited during β -cell destruction induced by STZ, such as interleukin 1 β , interferon- γ , and tumor necrosis factor- α (26), which could conceivably activate or sensitize some α -cell ion channels. In fact, several reports have shown that in colitis and ileitis animal models, release of inflammatory cytokine is associated with hyperexcitability of colonic dorsal root ganglion neurons, which were attributed to alterations in K_V and Na⁺ currents (31–35). These findings are consistent with our findings in α cells in the STZ-induced diabetes mouse model. Diabetes development in the STZ-treated mouse model (8) or in patients with T1D (36) is associated with similar inflammatory processes in the islets (i.e., insulinitis), wherein cytotoxic T cells are recruited and release inflammatory cytokines (26) that can be predicted to perturb ion channels in α cells, perhaps in a manner similarly observed in this study.

The STZ-induced diabetes animal model in several respects mimics human T1D. STZ is transported into the β cell through Glut2 transporters, inducing cytotoxicity by oxidative damage and autoimmune reaction (8), including lymphocyte infiltration leading to insulinitis and β -cell apoptosis (9). Because α cells express only Glut1 or Glut5 transporters (37,38), they are likely protected from STZ-mediated destruction, hence, the normal α -cell mass observed in this study. Furthermore, the complement of ion channel expression and functional properties of α cells in STZ-treated mice was comparable with α cells from control mice. Nevertheless, additional models of T1D, including noninflammatory (genetic ablation of β cells) (20) and autoimmune inflammatory (NOD mouse) models, should be tested in future studies to further validate the findings presented in this study and to explore the contributions of paracrine and inflammatory factors that may contribute to the perturbation of α cells in T1D. Insights from such studies could lead to strategies to correct such perturbation, thereby normalizing α -cell glucagon secretory responses (39).

ACKNOWLEDGMENTS

This study was mainly supported by the Canadian Diabetes Association (OG-3-10-3020-HG to H.Y.G.) and by a Canadian Institutes of Health Research doctoral award (CGD 76317 to Y.-C.H.). Z.-P.F. holds a Heart and Stroke Foundation New Investigator Award. This work is also supported by Juvenile Diabetes Research Foundation Project Grant 2007-685 to P.G. and by Slovenian Research Agency Programme P3-0310-2334, grant J3-2290-2334, and MPG Partner Group Programme to M.R.

No potential conflicts of interest relevant to this article were reported.

Y.-C.H. performed all the experiments and data analysis, designed experiments, and wrote the manuscript. M.S.R. and Z.-P.F. contributed to the design of some experiments and to discussion and reviewed and edited the manuscript. N.K. provided technical assistance in glucagon secretion assay. P.L.H. and P.G. contributed to the discussion and provided the mice. H.Y.G. is the guarantor of this work and, as such, had full access to all the data in the study and takes responsibility for the integrity of the data and the accuracy of the data analysis.

REFERENCES

- Dunning BE, Gerich JE. The role of alpha-cell dysregulation in fasting and postprandial hyperglycemia in type 2 diabetes and therapeutic implications. *Endocr Rev* 2007;28:253–283
- Quesada I, Tuduri E, Ripoll C, Nadal A. Physiology of the pancreatic alpha-cell and glucagon secretion: role in glucose homeostasis and diabetes. *J Endocrinol* 2008;199:5–19
- Cryer PE. Hypoglycaemia: the limiting factor in the glycaemic management of Type I and Type II diabetes. *Diabetologia* 2002;45:937–948
- Butler PC, Rizza RA. Contribution to postprandial hyperglycemia and effect on initial splanchnic glucose clearance of hepatic glucose cycling in glucose-intolerant or NIDDM patients. *Diabetes* 1991;40:73–81
- Gerich JE. Lilly lecture 1988. Glucose counterregulation and its impact on diabetes mellitus. *Diabetes* 1988;37:1608–1617
- Huang YC, Rupnik M, Gaisano HY. Unperturbed islet α -cell function examined in mouse pancreas tissue slices. *J Physiol* 2011;589:395–408
- Ramracheya R, Ward C, Shiget M, et al. Membrane potential-dependent inactivation of voltage-gated ion channels in alpha-cells inhibits glucagon secretion from human islets. *Diabetes* 2010;59:2198–2208
- Like AA, Rossini AA. Streptozotocin-induced pancreatic insulinitis: new model of diabetes mellitus. *Science* 1976;193:415–417
- O'Brien BA, Harmon BV, Cameron DP, Allan DJ. Beta-cell apoptosis is responsible for the development of IDDM in the multiple low-dose streptozotocin model. *J Pathol* 1996;178:176–181
- Quoix N, Cheng-Xue R, Guiot Y, Herrera PL, Henquin JC, Gilon P. The GluCre-ROSA26EYFP mouse: a new model for easy identification of living pancreatic alpha-cells. *FEBS Lett* 2007;581:4235–4240
- Anderson MS, Bluestone JA. The NOD mouse: a model of immune dysregulation. *Annu Rev Immunol* 2005;23:447–485
- Wang Q, Brubaker PL. Glucagon-like peptide-1 treatment delays the onset of diabetes in 8 week-old db/db mice. *Diabetologia* 2002;45:1263–1273
- Kwan EP, Gaisano HY. Glucagon-like peptide 1 regulates sequential and compound exocytosis in pancreatic islet beta-cells. *Diabetes* 2005;54:2734–2743
- Andersson SA, Pedersen MG, Vikman J, Eliasson L. Glucose-dependent docking and SNARE protein-mediated exocytosis in mouse pancreatic alpha-cell. *Pflugers Arch* 2011;462:443–454
- Gustavsson N, Wei SH, Hoang DN, et al. Synaptotagmin-7 is a principal Ca²⁺ sensor for Ca²⁺-induced glucagon exocytosis in pancreas. *J Physiol* 2009;587:1169–1178
- Quoix N, Cheng-Xue R, Mattart L, et al. Glucose and pharmacological modulators of ATP-sensitive K⁺ channels control [Ca²⁺]_i by different mechanisms in isolated mouse alpha-cells. *Diabetes* 2009;58:412–421
- Spigelman AF, Dai X, MacDonald PE. Voltage-dependent K(+) channels are positive regulators of alpha cell action potential generation and glucagon secretion in mice and humans. *Diabetologia* 2010;53:1917–1926
- Leung YM, Ahmed I, Sheu L, Tsushima RG, Diamant NE, Gaisano HY. Two populations of pancreatic islet alpha-cells displaying distinct Ca²⁺ channel properties. *Biochem Biophys Res Commun* 2006;345:340–344
- Leung YM, Ahmed I, Sheu L, et al. Electrophysiological characterization of pancreatic islet cells in the mouse insulin promoter-green fluorescent protein mouse. *Endocrinology* 2005;146:4766–4775
- Thorel F, Népoté V, Avril I, et al. Conversion of adult pancreatic alpha-cells to beta-cells after extreme beta-cell loss. *Nature* 2010;464:1149–1154
- Göpel SO, Kanno T, Barg S, Weng XG, Gromada J, Rorsman P. Regulation of glucagon release in mouse -cells by KATP channels and inactivation of TTX-sensitive Na⁺ channels. *J Physiol* 2000;528:509–520
- Hille B, Hille B. *Ion Channels of Excitable Membranes*. Sunderland, MA, Sinauer, 2001
- Braun M, Ramracheya R, Bengtsson M, et al. Voltage-gated ion channels in human pancreatic beta-cells: electrophysiological characterization and role in insulin secretion. *Diabetes* 2008;57:1618–1628
- Houamed KM, Sweet IR, Satin LS. BK channels mediate a novel ionic mechanism that regulates glucose-dependent electrical activity and insulin secretion in mouse pancreatic β -cells. *J Physiol* 2010;588:3511–3523
- Barg S, Galvanovskis J, Göpel SO, Rorsman P, Eliasson L. Tight coupling between electrical activity and exocytosis in mouse glucagon-secreting alpha-cells. *Diabetes* 2000;49:1500–1510
- Atkinson MA, Bluestone JA, Eisenbarth GS, et al. How does type 1 diabetes develop?: the notion of homicide or β -cell suicide revisited. *Diabetes* 2011; 60:1370–1379
- Wendt A, Birnir B, Buschard K, et al. Glucose inhibition of glucagon secretion from rat alpha-cells is mediated by GABA released from neighboring beta-cells. *Diabetes* 2004;53:1038–1045

28. Xu E, Kumar M, Zhang Y, et al. Intra-islet insulin suppresses glucagon release via GABA-GABAA receptor system. *Cell Metab* 2006;3:47–58
29. Zhou H, Tran PO, Yang S, et al. Regulation of alpha-cell function by the beta-cell during hypoglycemia in Wistar rats: the “switch-off” hypothesis. *Diabetes* 2004;53:1482–1487
30. Zhou H, Zhang T, Harmon JS, Bryan J, Robertson RP. Zinc, not insulin, regulates the rat alpha-cell response to hypoglycemia in vivo. *Diabetes* 2007;56:1107–1112
31. Ibeakanna C, Vanner S. TNFalpha is a key mediator of the pronociceptive effects of mucosal supernatant from human ulcerative colitis on colonic DRG neurons. *Gut* 2010;59:612–621
32. Beyak MJ, Ramji N, Krol KM, Kawaja MD, Vanner SJ. Two TTX-resistant Na⁺ currents in mouse colonic dorsal root ganglia neurons and their role in colitis-induced hyperexcitability. *Am J Physiol Gastrointest Liver Physiol* 2004;287:G845–G855
33. Beyak MJ, Vanner S. Inflammation-induced hyperexcitability of nociceptive gastrointestinal DRG neurones: the role of voltage-gated ion channels. *Neurogastroenterol Motil* 2005;17:175–186
34. King DE, Macleod RJ, Vanner SJ. Trinitrobenzenesulphonic acid colitis alters Na⁺ 1.8 channel expression in mouse dorsal root ganglia neurons. *Neurogastroenterol Motil* 2009;21:880–e64
35. Stewart T, Beyak MJ, Vanner S. Ileitis modulates potassium and sodium currents in guinea pig dorsal root ganglia sensory neurons. *J Physiol* 2003;552:797–807
36. Walker JN, Johnson PR, Shigeto M, Hughes SJ, Clark A, Rorsman P. Glucose-responsive beta cells in islets isolated from a patient with long-standing type 1 diabetes mellitus. *Diabetologia* 2011;54:200–202
37. Heimberg H, De Vos A, Pipeleers D, Thorens B, Schuit F. Differences in glucose transporter gene expression between rat pancreatic alpha- and beta-cells are correlated to differences in glucose transport but not in glucose utilization. *J Biol Chem* 1995;270:8971–8975
38. Sato Y, Ito T, Udaka N, et al. Immunohistochemical localization of facilitated-diffusion glucose transporters in rat pancreatic islets. *Tissue Cell* 1996;28:637–643
39. Zhou H, Zhang T, Oseid E, Harmon J, Tonooka N, Robertson RP. Reversal of defective glucagon responses to hypoglycemia in insulin-dependent autoimmune diabetic BB rats. *Endocrinology* 2007;148:2863–2869